Thin Solid Films 531 (2013) 332–339

Contents lists available at SciVerse ScienceDirect

Thin Solid Films

journal homepage: www.elsevier.com/locate/tsf

Failure and debonding of thin circular and square tiles (islands) bonded with a compliant interlayer

Matthew R. Begley [a,b,*], Frank Zok [b], Natasha Vermaak [c]

[a] Mechanical Engineering Department, 2361 Engineering II Building, University of California, Santa Barbara, CA 93106, USA
[b] Materials Department, 1331 Engineering II Building, University of California, Santa Barbara, CA 93106, USA
[c] SIMaP-Universite de Grenoble, UMR 5266 CNRS/INPG/UJF, 1130 rue de la Piscine B.P. 75, F-38402 St. Martin dHeres Cedex, France

ARTICLE INFO

Article history:
Received 21 June 2012
Received in revised form 22 November 2012
Accepted 26 November 2012
Available online 19 December 2012

Keywords:
Delamination
Yielding
Island
Tile
Reliability

ABSTRACT

This paper presents analytical solutions for the stresses in circular thin films bonded to a substrate with a thin compliant interlayer. The axisymmetric results are shown to be an excellent approximation for square tiles (islands), provided one defines an effective diameter equal to the average of the square's diagonal and width. An analytical result is also presented for the energy release rate associated with convergent circular delamination cracks (from the outer edges of the tile inwards). These solutions are used to generate regime maps that indicate active failure mechanisms (tile yielding, interlayer yielding and delamination) as a function of constituent properties and tile size. These regime maps clearly indicate acceptable tile sizes and/or the required material properties to avoid all modes of failure.

1. Introduction

A wide variety of technologies involve the use of tile-like structures (often referred to as "islands") bonded to substrates, as shown schematically in Fig. 1. Examples include sensor arrays, displays, microelectronic packaging and thermal protection systems (e.g. [1–10,12–14]). Interlayers are commonly present between the tiles and the substrate to promote adhesion and/or to provide thermal or electrical insulation. The relationship between stresses arising from thermal expansion mismatch and tile size plays a critical role in design, as it ultimately governs the susceptibility of the system to failure by yielding, cracking or interfacial debonding (e.g. [11,13,12,14,15]).

As is well-known from shear lag theory [16], the in-plane direct stress in a tile due to a misfit strain increases from the outer edge towards the center, a consequence of the shear transfer between the tile and the underlying structure (e.g. [16–25]). (Note that many of these and other references address the problem of multiple cracking in blanket films, which leads to thin strips of finite dimension; the crack spacing dictates the tile or island size.) The peak stress at the tile center depends on the tile size relative to a characteristic shear transfer length, and asymptotically approaches the blanket-film result in the limit of large tile sizes. Even for applications where finite-sized features are not a prerequisite (e.g. a thermal protection system that has no inherent constraint on planar dimension), the stresses in large tiles may be too high to avoid failure. In such scenarios, the use of finite-sized tiles can be an effective way to reduce stresses and improve reliability (e.g. [11,13,12,14,15]).

Hence, a central design variable for such systems is the tile size. A maximum allowable size might be prescribed in order to avoid failure, given a pre-determined set of thermomechanical properties for the constituents. Alternatively, if the tile size is fixed by other considerations (e.g. sensor area), one might pose the question in terms of an acceptable range of properties (such as adhesion or coefficient of thermal expansion (CTE) mismatch). In such design exercises, closed-form relationships between geometry, properties and stress are highly advantageous, in that they eliminate the need for cumbersome numerical studies of the parameter space. This is particularly true for applications in which material selection is part of the design process (as opposed to being fixed a priori), since there are likely many possible combinations of materials and tile sizes that are acceptable.

Here, we present closed-form solutions for deformations and stresses in a thin circular tile mounted on a thick substrate via a compliant interlayer. The solutions are shown to be accurate approximations for square tiles, subject to a suitable definition for the effective tile diameter. In turn, the stress solutions are used to estimate the steady-state energy release rates for interlayer debonding. The steady-state energy release rate corresponds to the maximum possible driving force, obtained when the crack length is much greater than the tile thickness (e.g. [26,27] and references therein). Previous calculations have demonstrated that the energy release rate grows quickly as a function of crack length, reaching steady state for lengths (measured from the outer edge

* Corresponding author. Tel.: +1 805 679 1122.
E-mail address: begley@engr.ucsb.edu (M.R. Begley).

0040-6090/$ – see front matter © 2013 Elsevier B.V. All rights reserved.
http://dx.doi.org/10.1016/j.tsf.2012.11.136

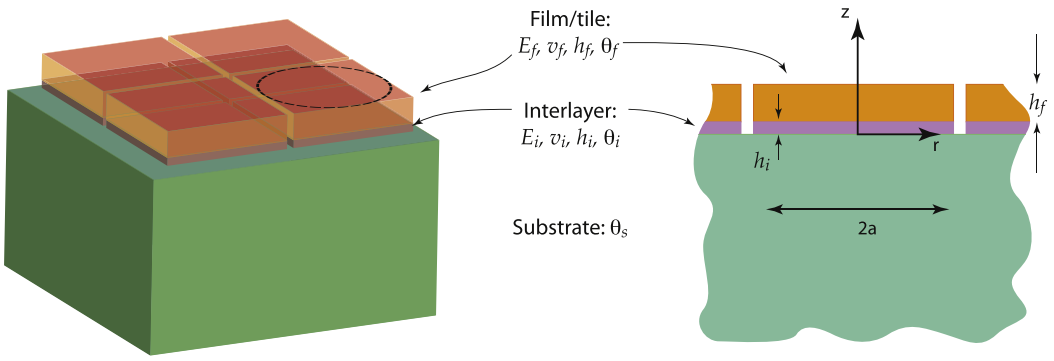

Fig. 1. Schematic of the tiling system. The problem is analyzed as axisymmetric, with the tile (island) diameter denoted as a. It is shown via comparison with finite element analysis (FEA) of square tiles that the axisymmetric model is accurate provided the effective radius is taken $a = (1/4)\left(w + \sqrt{2}w\right)$, where w is the width of the square tile.

of the tile) on the order of several tile thicknesses [25–27]. The resulting solutions for stresses and energy release rates are then used to construct regime maps that facilitate design of tiling systems. The maps depict various failure modes (yielding, cracking or interface debonding) in terms of system geometry (characterized by layer thicknesses and tile size) and material properties (e.g. stiffness, yield strength, thermal expansion and toughness).

Though this analysis is inspired by and resembles a variety of previous shear-lag analyses of stress and debonding in finite-sized features [16–25,28–31], a critical distinguishing feature of the present work is the treatment of the in-plane tile stresses acting parallel to the free edges. Here, these stresses are non-zero and dictated by the tile size. Previous treatments that assume plane-strain deformation (i.e. a semi-infinite strip) or purely biaxial deformation lead to inappropriate predictions of direct stress in the direction parallel to the free edge. That is, if one assumes purely biaxial stress and imposes the condition that the in-plane stresses are zero at the free edge, then the stress parallel to the free edge is assumed to be zero, which is not the case. Similarly, if one assumes plane-strain deformation of a semi-infinite strip, then the stress parallel to the free edge is not a function of tile size, which is not the case. The present model properly imposes the condition that the stress along the edges is zero in the direction normal to the surface, and dictated by the tile size in the direction parallel to the edge. Further, the model enables failure maps that indicate transitions in failure mechanism as a function of tile size and key dimensionless parameters identified here. As with all shear-lag analyses, the model assumes that displacements occur only in the plane of the tile, such that through-thickness effects are negligible. In order for this to be valid, the aspect ratio of the tiles (planar dimension divided by the total thickness) must be large. It is further assumed that the tiling system is attached to a substrate that is much thicker than the top layers, such that bending in the multilayer is negligible.

2. Model and results

The constituents are assumed to be linearly elastic with the properties: E-Young's modulus, v-Poisson's ratio and h-thickness. The substrate is assumed to be semi-infinite, such that bending deformation is negligible. This implies that the stress in the tile scales with the misfit strain given by θ_s–θ_f, where $\theta_{s,f}$ are the eigenstrains in the substrate and film (top tile). (For example, for thermal misfit, $\theta = \alpha\Delta T$, where α—CTE, and $\Delta T = T - T^o$ is the temperature change relative to the stress-free reference temperature T^o). Subscripts refer to a specific layer: f-film (or tile), s-substrate, and i-interlayer. The analysis assumes that the majority of deformation in the tile is axisymmetric, with only radial displacements being non-zero. It is demonstrated that this is an accurate approximation for square tiles, with minor deviations near the tile corners that are not likely to impact design choices.

2.1. Shear lag analysis and displacement solution

The model assumes only radial displacements, $u(r)$, such that the kinematic and constitutive relationships for the film are given by:

$$\epsilon_r = \frac{\partial u(r)}{\partial r}; \frac{\left(1-v_f^2\right)\sigma_r^f}{E_f} = \epsilon_r + v_f\epsilon_\theta - \left(1+v_f\right)\theta_f \tag{1}$$

$$\epsilon_\theta = \frac{u(r)}{r}; \frac{\left(1-v_f^2\right)\sigma_\theta^f}{E_f} = \epsilon_\theta + v_f\epsilon_r - \left(1+v_f\right)\theta_f. \tag{2}$$

Equilibrium in the film dictates the following:

$$\frac{\partial\sigma_r^F}{\partial r} + \frac{\sigma_r^f - \sigma_\theta^f}{r} + \frac{\partial\sigma_{rz}^f}{\partial z} = 0. \tag{3}$$

In the present approximation, the shear stress in the thin interlayer, σ_{rz}^i, is assumed to be uniform through its thickness, and governed by the difference of the displacements at the top and bottom of the interlayer:

$$\sigma_{rz}^i = \frac{E_i}{2(1+v_i)}\left(\frac{u(r)-\theta_s r}{h_i}\right), \tag{4}$$

where $u(r)$ is the displacement of the top of the interlayer, which is equal to the film displacement. The quantity $\theta_s r$ reflects the uniform outward expansion of the bottom of the interlayer due to the substrate's expansion. In this regard, the effect of mechanical stretching of the substrate can be easily accounted for by including the imposed strain in the definition of θ_s, as in $\theta_s = \alpha_s\Delta T_s + \epsilon_a$, where ϵ_a is the strain applied to the substrate. The shear stress in the film at the interface acts opposite to that in the interlayer (as defined above); further, the shear stress is zero at the top of the film. Assuming that the film is thin, the gradient of shear stress in the film is well-approximated by:

$$\frac{\partial\sigma_{rz}^f}{\partial z} \approx -\frac{\sigma_{rz}^i}{h_f} = \frac{E_i}{2(1+v_i)}\left(\frac{u(r)-\theta_s r}{h_i h_f}\right). \tag{5}$$

The governing equation for radial displacements is obtained by combining Eqs. (1)–(5). Using the normalizations $u = a\cdot\bar{u}$ and $r = a\cdot\bar{r}$, where a is the tile radius, one obtains the following governing equation:

$$\bar{u}'' + \frac{\bar{u}'}{\bar{r}} - \frac{\bar{u}}{\bar{r}^2} - \lambda^2(\bar{u} - \theta_s\cdot\bar{r}) = 0 \tag{6}$$

where

$$\lambda = \frac{a}{a_o} = \sqrt{\frac{\left(1-\nu_f^2\right)E_i a^2}{2(1+\nu_i)E_f h_i h_f}}; a_o = \sqrt{\frac{2(1+\nu_i)E_f h_i h_f}{\left(1-\nu_f^2\right)E_i}}. \quad (7)$$

The parameter λ is thus a ratio of the size of the tile to a characteristic length-scale describing the shear transfer length between the tile and the interlayer, i.e. $\lambda = a/a_o$.

The boundary conditions are $\bar{u}(0)=0$ and $\sigma_r^f(1)=0$, i.e. zero displacement at the center of the tile and zero normal stresses acting at the outer edge of the tile. With these conditions, the radial displacement along the interface is given by:

$$\bar{u}(\bar{r}) = \theta_s \cdot \bar{r} + \left(1+\nu_f\right)\left(\theta_f - \theta_s\right)\frac{I_1[\lambda\cdot\bar{r}]}{\lambda I_0[\lambda] - \left(1-\nu_f\right)I_1[\lambda]}, \quad (8)$$

where I_n are modified Bessel functions of the first kind. This solution can be used to derive the stress distributions, which are presented in the next section. Note that $\bar{u}(1)$ is an important result in its own right, since the displacement of the edge of the tile determines whether an initial gap between the tiles closes.

2.2. Tile stresses

The stresses are found via Eq. (8) with Eqs. (1) and (2). The key scaling factor that emerges is simply the biaxial stress in an infinitely large island:

$$\sigma_o = \frac{E_f}{1-\nu_f}\left(\theta_s - \theta_f\right). \quad (9)$$

Using this definition, the dimensionless radial and circumferential stress distributions in the tile are given by:

$$\bar{\sigma}_r^f = \frac{\sigma_r^f}{\sigma_o} = \frac{\lambda\cdot\bar{r}\cdot I_o[\lambda] - \lambda\cdot\bar{r}\cdot I_o[\lambda\cdot\bar{r}] - \left(1-\nu_f\right)(\bar{r}\cdot I_1[\lambda] - I_1[\lambda\cdot\bar{r}])}{\lambda\cdot\bar{r}\cdot I_o[\lambda] - \left(1-\nu_f\right)\cdot\bar{r}\cdot I_1[\lambda]} \quad (10)$$

$$\bar{\sigma}_\theta^f = \frac{\sigma_\theta^f}{\sigma_o} = \frac{\lambda\cdot\bar{r}\cdot I_o[\lambda\cdot\bar{r}] - \nu_f\cdot\lambda\cdot\bar{r}\cdot I_o[\lambda] + \left(1-\nu_f\right)(\bar{r}\cdot I_1[\lambda] - I_1[\lambda\cdot\bar{r}])}{\lambda\cdot\bar{r}\cdot I_o[\lambda] - \left(1-\nu_f\right)\cdot\bar{r}\cdot I_1[\lambda]}. \quad (11)$$

Representative illustrations of the stress distributions are given in Fig. 2A. Note that the radial stress is zero at the outer edge, while the circumferential stress (parallel to the outer edge) is not zero. The direction stresses are equal and maximum at the center of the tile:

$$\bar{\sigma}_r^{max} = \bar{\sigma}_\theta^{max} = \bar{\sigma}_{VM}^{max} = 1 - \frac{\left(1+\nu_f\right)\lambda}{2\lambda I_o[\lambda] - 2\left(1-\nu_f\right)I_1[\lambda]} \quad (12)$$

where *VM* refers to the Von Mises stress. This provides the basis to predict tile yielding. The peak stress is shown in Fig. 2B as a function of normalized tile size. For large tile sizes, the stresses asymptote to the biaxial result, as expected. When the tile size is comparable to the shear transfer length, the stresses are reduced because the tile is not large enough to build significant stresses through shear of the interlayer.

An important feature of the solution is the fact that the direct stress in the tile decreases with tile size much faster than the shear stress in the interlayer. For example, as shown in Fig. 2B for the tile size $a = a_o$ (i.e. $\lambda = 1$), the direct stresses in the tile have been reduced by 75%, while the shear stress in the interlayer has been reduced by only 40%. This implies that as the tile size is decreased relative to a_o, interlayer yielding becomes more of a concern than debonding or tile yielding. (Look ahead to Fig. 4.)

A somewhat simpler but nearly identical result can be derived by assuming that the two in-plane stresses are identical throughout the tile; repeating the shear lag analysis under these assumptions yields:

$$\bar{\sigma}_{VM}^{max} \approx 1 - \frac{1}{\cosh[\lambda_e]}; \quad \lambda_e = \left(\frac{2}{1+\sqrt{2}}\right)\lambda \quad (13)$$

where λ_e is an effective tile size obtained by dividing the average of the edge and corner distances. That is, analyzing a square tile under the assumption of purely biaxial stress yields nearly equivalent results to the present analysis provided the tile size is defined as *the effective tile size given above. The effective tile size is simply a slight modification to the actual tile size to obtain agreement between purely biaxial analysis and the axisymmetric analysis*. Note that this approximation only yields accurate results for the maximum stress, since the bi-axial approximation enforces the condition that both stresses are zero at the tile edges, which is not the case. For this reason, a purely biaxial analysis will yield energy release rates that are not accurate.

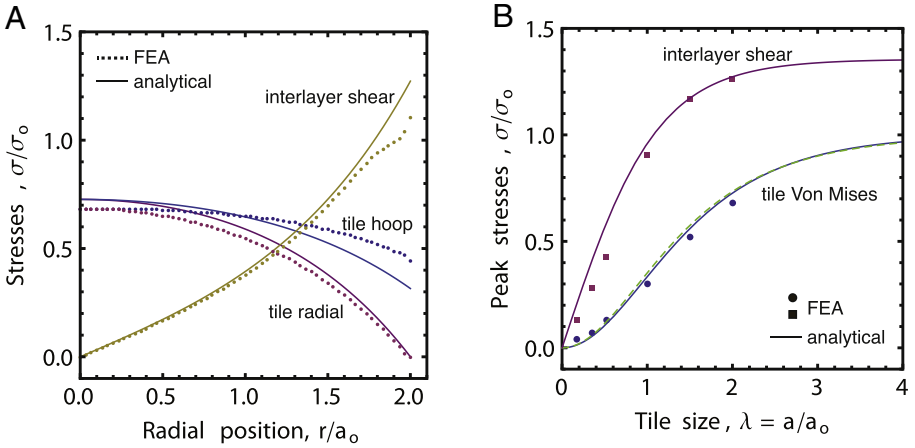

Fig. 2. (A) Stresses distributions in the tile for $\nu_f = 1/3$ and the tile size $\lambda = a/a_o = 2$. The dots represent the results of finite element analysis (FEA). The interlayer shear stress has an additional scaling factor such that the curve represents $a\sigma_{rz}/(h_f\sigma_o)$. (B) The peak stress in the tile (center) and interlayer (edge) as a function of tile size: the dots represent the results of the finite element analysis, with the peak interlayer shear stress chosen as the value h_i from the edge. To get accurate results for square tiles, the effective radius should be taken as $a = (1/4)\left(w + \sqrt{2}w\right)$, where w is the square tile size. The dashed green curve represents the purely biaxial approximation discussed in the text.

To evaluate the accuracy of the model, three-dimensional finite element calculations were conducted on tile systems with different values of a_o. The finite element results are shown in Fig. 2 along with the model predictions. Excellent agreement between the numerical and analytical results is seen for $\lambda = a/a_o > \approx 0.4$. The agreement is better for stresses at the center of the tile than for the interlayer shear stress, likely due to edge effects not accounted for in the analytical model. Strictly speaking, there is a (usually weak) corner singularity in the interlayer at the tile edge: the reported values correspond to distances that are one interlayer thickness inside the outer edge.

It should be kept in mind that the shear lag approximation assumes that the tile size is large in comparison to the interlayer or tile thickness. Otherwise, the stress state in the tile cannot be idealized as one-dimensional. This implies that the shear-lag will not be accurate for small values of λ. As illustrated in subsequent sections, the shear lag model produces reasonable results for $a/h_f > \approx 5$. Taking this as a rule of thumb, the minimum value of λ for which one expects the shear-lag approximation to be valid is given by:

$$\lambda_{min} \approx 5\sqrt{\frac{\left(1-\nu_f^2\right)E_i h_f}{2(1+\nu_i)E_f h_i}}. \tag{14}$$

2.3. Interlayer stresses

The shear stress distribution in the interlayer can be calculated from Eq. (4) using Eq. (8), and is given by:

$$\sigma_{rz}^i = \frac{E_i a\left(1+\nu_f\right)\left(\theta_f-\theta_s\right)}{2(1+\nu_i)h_i}\frac{I_1[\lambda\cdot\bar{r}]}{\lambda I_0[\lambda]-\left(1-\nu_f\right)I_1[\lambda]}. \tag{15}$$

The maximum occurs at the edge of the tile ($\bar{r}=1$). Dividing by the characteristic stress in the *tile*, σ_o, the normalized peak shear stress is given by:

$$\hat{\sigma}_{rz}^i = \frac{a_o}{h_f}\frac{\sigma_{rz}^f}{\sigma_o} = \frac{\lambda\cdot I_1[\lambda]}{\lambda\cdot I_o[\lambda]-\left(1-\nu_f\right)I_1[\lambda]}, \tag{16}$$

where $\hat{}$ indicates the different normalization as compared to the tile stresses. The pre-factor in Eq. (14) illustrates that an additional scaling factor (other than a/a_o and σ_o) factors into the shear stress in the interlayer, i.e. a_o/h_f.

In the following discussion, direct stresses in the interlayer are neglected. In reality, the direct stresses in the interlayer build from the edges according to the exact same shear transfer mechanism as above, only with the shear stress at the interlayer/substrate interface generating the direct stresses. Using the same argument as above, one expects the direct stresses to build in the interlayer according to a dimensionless size parameter given by:

$$\lambda_{is} = \sqrt{\frac{(1-\nu_i)E_s a^2}{2(1+\nu_s)E_i h_i h_s}}. \tag{17}$$

When this parameter is small (which notably occurs for thick substrates), shear transfer between the interlayer and substrate occurs over much smaller distances than the tile size, such that the stresses in the majority of the interlayer are given by the blanket film result:

$$\sigma_{r,\theta}^i = \frac{E_i(\theta_s-\theta_i)}{1-\nu_i}. \tag{18}$$

2.4. Energy release rates for debonding

Here, we assume that an interface crack grows from the outer edge of the tile inwards, leaving a circular patch that remains bonded. It is assumed that the debonded length is much greater than a_o, i.e. the length-scale associated with shear transfer, such that edge effects are negligible. The stresses in the released bilayer outside the crack front are taken to be zero since the released section is free to expand. Strictly speaking, this is not true, as (1) debonding will not release circumferential stress immediately in the crack wake, and (2) the bilayer may have retained stresses due to tile/interlayer mismatch. However, the current approximation is conservative in that it overestimates the amount of strain energy released by debonding.

In this scenario, the energy release rate for debonding is simply the reduction in strain energy that results from a decrease in the size of the bonded patch:

$$\mathrm{G} = \frac{1}{2\pi a}\frac{\partial\left(\Phi_f+\Phi_i\right)}{\partial^{\mathrm{a}}}, \tag{19}$$

where Φ_f is the strain energy in the tile and Φ_i is the strain energy in the interlayer. Here, we assume that debonding releases the strain energy in the interlayer associated with shear-transfer. Direct stresses in the interlayer do not affect debonding between the tile and the interlayer, as they would not be released by debonding above the interlayer. However, if one considers debonding between the interlayer and substrate, the strain energy associated with these direct stresses should be included, as it would increase the driving force for debonding.

In terms of the normalized tile size $\lambda = a/a_o$, a suitable normalized energy release rate is given by:

$$\bar{G} = \frac{G}{G_o} = \frac{1}{2\pi\lambda}\frac{\partial\left(\bar{\Phi}_f+\bar{\Phi}_i\right)}{\partial\lambda} \tag{20}$$

where G_o is the strain energy density per unit thickness of the tile, given by:

$$G_o = \frac{\left(1-\nu_f\right)\sigma_o^2 h_f}{2E_f}, \tag{21}$$

$\bar{\Phi}_f = \bar{\Phi}_f/\left(G_o a_o^2\right)$ and $\bar{\Phi}_i = \Phi_i/\left(G_o a_o^2\right)$. According to the present assumptions, G_o is the energy release rate for debonding in the limit of infinite tile size, i.e. large values of λ. This is higher by a factor of $(1+\nu_f)$ than the classical result for plane strain debonding that does not release stresses parallel to the crack front, which illustrates that the estimate is conservative.

Using these definitions, the *total* strain energy in the tile where the interface is bonded is given by:

$$\begin{aligned}\bar{\Phi}_f &= \frac{2E_f\Phi_f}{\left(1-\nu_f\right)\sigma_o^2 h_f a_o^2}\\ &= \frac{2\pi\cdot\lambda^2}{1-\nu_f}\int_0^1\left[\left(1+\nu_f\right)\left(\bar{\sigma}_r^2+\bar{\sigma}_\theta^2\right)-\nu_f(\bar{\sigma}_r+\bar{\sigma}_\theta)^2\right]\cdot\bar{r}\cdot d\bar{r},\end{aligned} \tag{22}$$

where the dimensionless stresses are given above. The total strain energy in the interlayer is given by:

$$\bar{\Phi}_i = \frac{2E_f\Phi i}{\left(1-\nu_f\right)\sigma_o^2 h_f a_o^2} = 2\pi\left(1-\nu_f\right)\cdot\lambda^2\int_0^1\hat{\sigma}_{rz}^2\cdot\bar{r}\cdot d\bar{r}, \tag{23}$$

where it should be noted that $\hat{\sigma}_{rz}$ is defined such that it is only a function of λ. Hence, the strain energy in the interlayer depends only on the variables $\Phi_f(\nu_f,\lambda)$, and thus scales with the interlayer properties

only through the dimensionless size λ. This is important to note because it implies that the strain energy in the interlayer cannot be neglected purely on the basis that it may be much thinner or more compliant than the film.

Thus, the normalized strain energy release rate can be computed using Eq. (18) with Eqs. (20) and (21), after substituting Eqs. (10), (11) and (14) for the stresses. It is instructive to separate the total energy release into contributions arising from the tile and from the interlayer, i.e. $\bar{G} = \bar{G}_f + \bar{G}_i$, where the components are simply the terms corresponding to the derivatives of each strain energy term:

$$\bar{G}_f = \frac{c_1 I_o^3 + c_2 I_1 I_o^2 + c_3 I_1 I_o^2 + c_4 I_1^3}{2\left(\lambda I_o - \left(1-\nu_f\right) I_1\right)^3} \tag{24}$$

$$c_1 = \left(1-\nu_f\right)\left(2+\nu_f\right)\lambda^3 \tag{25}$$

$$c_2 = \lambda\left(-12\left(-1+\nu_f\right) + \lambda^2\left(1+\nu_f\right)^2\right) \tag{26}$$

$$c_3 = \lambda^2\left(-\lambda^2\left(1+\nu_f\right) + 3\left(-1+\nu_f\right)\left(3+\nu_f\right)\right) \tag{27}$$

$$c_4 = -4 + 2\lambda^2 + \lambda^4 + \nu_f\left(8 + \lambda^4 - 2\left(2+\lambda^2\right)\nu_f\right) \tag{28}$$

$$\bar{G}_i = \frac{b_1 I_1 I_o^2 + b_2 I_1^3 + b_3 I_o^3 + b_4 I_1^2 I_o}{\left(\lambda I_o - \left(1-\nu_f\right) I_1\right)^3} \tag{29}$$

$$b_1 = \lambda^2\left(4 + \lambda^2 - 4\nu_f\right)\left(1+\nu_f\right)^3 \tag{30}$$

$$b_2 = \lambda^2\left(-12\left(-1+\nu_f\right) + \lambda^2\left(1+\nu_f\right)^2\right) \tag{31}$$

$$b_3 = \lambda^3\left(-1+\nu_f\right)\left(1+\nu_f\right)^3 \tag{32}$$

$$b_4 = \lambda\left(1+\nu_f\right)^3\left(4 + \left(-4+\lambda^2\right)\nu f\right) \tag{33}$$

where I_o and I_1 are the modified Bessel's functions of the first kind, to be evaluated at λ.

Fig. 3 illustrates the energy release rate for debonding at the tile/interlayer interface as a function of tile size for $\nu_f = 1/3$: all other parameters are accounted for in the normalizations (i.e. G_o and a_o). It is interesting to note that the energy released by relaxation of the shear stresses in the interlayer is dominant for tile sizes less than $\lambda \sim 1$. This is because the peak shear stress in the interlayer decreases with tile size slower than the tile stress, as shown in Fig. 2B.

3. Failure mechanism maps

The present model enables the prediction of three different failure modes: (*i*) yielding of the tile, (*ii*) yielding of the interlayer, and (*iii*) tile/interlayer debonding. Here, we use σ_c to denote the critical value of $\sigma_o = E_f(\theta_s - \theta_f)/(1-\nu_f)$ that triggers failure. We present results wherein the critical value is scaled by the yield stress of the tile, σ_c/σ_Y. Hence, with regard to tile yielding, the quantity σ_c/σ_Y corresponds to the ratio of the allowable misfit strain to the biaxial yield strain, as in $(\theta_s - \theta_f)_c/\epsilon_Y$, where $\epsilon_Y \equiv (1-\nu_f)\sigma_Y/E_f$. With this normalization, the critical stress σ_c/σ_Y for tile yielding asymptotes to unity for large tile sizes; values above unity reflect the fractional gain in allowable misfit strains that arise from reducing the tile size.

To provide a common basis to compare critical thermal loads for each mechanism, the critical stresses corresponding to interlayer yielding and debonding are also normalized by σ_Y. The following

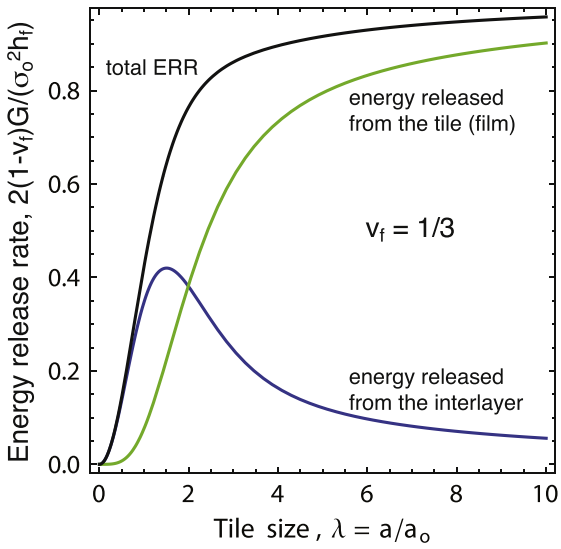

Fig. 3. Energy release rate (G/G_o) for debonding as a function of a tile size, $\lambda = a/a_o$, showing the contributions from the energy released in the interlayer and the energy released from the tile.

three dimensionless equations define the critical values of σ_o that trigger each mechanism:

$$\frac{\sigma_o^c}{\sigma_Y} = F_t\left(\lambda, \nu_f\right) \textit{tile yielding} \tag{34}$$

$$\frac{\sigma_o^c}{\sigma_Y} = \Sigma_R \cdot F_i\left(\lambda, \nu_f\right) \textit{interlayer yielding} \tag{35}$$

$$\frac{\sigma_o^c}{\sigma_Y} = \Gamma_R \cdot F_d\left(\lambda, \nu_f\right) \textit{debonding} \tag{36}$$

where the functions F_t and F_i are the reciprocals of the right-hand sides of Eqs. (12) and (16), respectively. $F_d = 1/\sqrt{\bar{G}}$, where $\bar{G}$ is defined via Eqs. (24)–(33). Σ_R and Γ_R are two dimensionless parameters that are functions of material properties, given as:

$$\Sigma_R = \frac{\tau_Y^i}{\sigma_Y}\sqrt{\frac{2(1+\nu_i)E_f h_i}{\left(1-\nu_f^2\right)E_i h_f}}, \tag{37}$$

$$\Gamma_R = \sqrt{\frac{2G_c E_f}{\sigma_Y^2 h_f}}. \tag{38}$$

Here, τ_Y^i is the yield stress in shear of the interlayer, such that Σ_R is a measure of the relative yield strengths of the interlayer and tile. G_c is the critical energy release rate for the interface between the tile and the interlayer, such that Γ_R is a measure of the interface's resistance to debonding relative to the tile yield strength. Thus, for all three mechanisms, the critical stress is only a function of $\sigma_c = f(\lambda, \Sigma_R, \Gamma_R, \nu_f)$. The dependence on the Poisson's ratio is rather weak: $\nu_f = 1/3$ is used to generate the illustrative results in this paper.

Fig. 4 illustrates the allowable tile stress σ_c/σ_Y as a function of tile size for several different values of the material parameters Σ_R and Γ_R. The trend of increasing critical stress with decreasing tile size is exhibited for all failure mechanisms, and is a consequence of the decrease in stress associated with the free edges of the tile. These figures illustrate that dramatic increases in critical stresses are possible by reducing the tile size. The kinks in the curves are a result of a transition in active failure mechanism. For example, in Fig. 4A, for $\Gamma_R = 1$ and $\Sigma_R = 1.5$, tile yield is the active constraint for $\lambda \gtrsim 3.5$, while interlayer yielding is active for smaller tile sizes. For values $\Sigma_R \lesssim 1.5$, interlayer

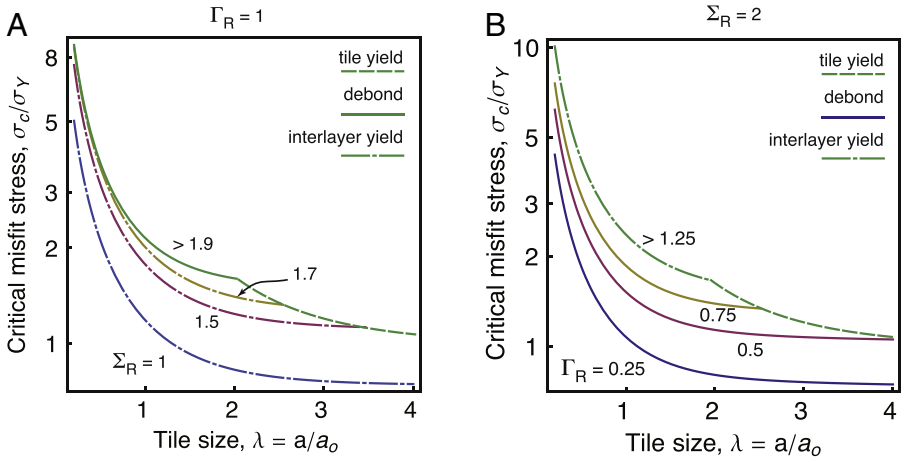

Fig. 4. Critical misfit stress σ_c/σ_Y as a function of tile size $\lambda = a/a_o$, determined by the minimum value required to trigger any mechanism. The toughness parameter is $\Gamma_R = \sqrt{\frac{2G_c E_f}{\sigma_Y^2 h_f}}$, while the strength parameter is $\Sigma_R = \frac{\tau_Y}{\sigma_Y}\sqrt{\frac{2(1+\nu_i)E_f h_i}{\left(1-\nu_f^2\right)E_i h_f}}$. The line pattern indicates the active failure mechanism at the critical misfit stress.

yielding occurs at the lowest misfit strain for all tile sizes, and hence no kink exists. Similarly, for $\Sigma_R \gtrsim 1.8$ and $\Gamma_R \lesssim 1$, the interlayer is strong enough such that interlayer yielding does not occur prior to either tile yielding or debonding. Similar transitions are seen in Fig. 4B; for low values of Γ_R, debonding is the active mechanism: once Γ_R is high enough (e.g. $\Gamma_R \gtrsim 1$ for $\Sigma_R = 2$), the critical stress is dictated by either tile yielding or interlayer yielding.

The trends in active failure mechanism as a function of tile size can be broadly illustrated by constructing a contour plot of the critical stress values as a function of λ and Γ_R, as shown in Fig. 5A, and λ and Γ_R, as shown in Fig. 5B. In both figures, the remaining material property is held constant. Naturally, the largest value of σ_c occurs at the smallest tile sizes. There is a narrow range of either Σ_R or Γ_R where all three failure mechanisms are possible: roughly, $1.7 \lesssim \Sigma_R \lesssim 2$ and $1 \lesssim \Gamma_R \lesssim 1.4$. If either material property falls out of this range, there are only two possible failure mechanisms for any tile size. For example, for $\Gamma_R \gtrsim 1.4$ and $\Sigma_R \lesssim 2$, the failure mechanism transitions from tile yielding at large tile sizes to interlayer yielding at smaller tile sizes. Similarly, for $\Sigma_R \gtrsim 2$ and $\Gamma_R \lesssim 1$, the failure mechanism transitions from tile yielding at large tile size to debonding at smaller tile size.

The material properties needed to avoid failure for a given tile size are illustrated in Fig. 6, which presents an alternative view of the (λ, Σ_R,Γ_R) design space. Here, the size is fixed to be $\lambda = 1.5$ while the other parameters are varied. In Fig. 6A, interlayer yielding (Σ_R) controls the critical stress until a critical value dictated by the interface toughness (Γ_R) is reached: once both parameters are large enough, tile yielding becomes the active mechanism (i.e. the plateau in Fig. 6A). Similarly, in Fig. 6B, interface toughness (Γ_R) controls strength until the mechanism switches over to interlayer yielding (i.e. Σ_R controlled). Again, when both properties are sufficiently large, tile yielding is the active constraint.

A central design exercise for tiling systems pertains to finding the maximum allowable tile size that will avoid failure, given minimum bounds on the material properties of the system (i.e. estimates for the lower bounds for Σ_R and Γ_R). Fig. 7 plots contours of the critical stress for two tile sizes as a function of (Σ_R,Γ_R). The critical stresses increase to a maximum at the intersection of the three constraints; the critical stress value at this intersection increases with decreasing tile size, as expected. Decreasing the tile size shifts the "tile yielding" plateau upwards and to the right, as seen by comparing Fig. 7A and B. This implies that, in order to realize the higher critical stress allowed for the given tile size, (i.e. utilize the increased range in misfit strains that are allowed) one must increase both material properties. Of course, if the tile size is decreased while the properties and critical stress are held fixed, the shift in the tile yielding region merely

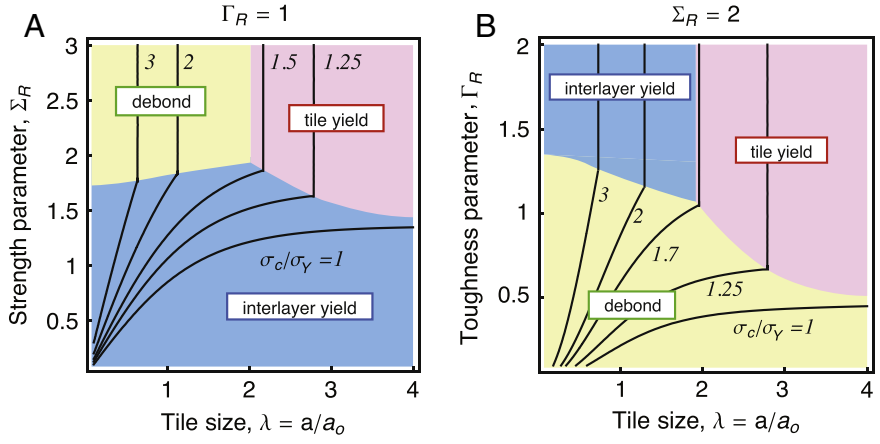

Fig. 5. Contours of the critical misfit stress, σ_o^c/σ_Y as a function of tile size $\lambda = a/a_o$ and the material parameters controlling various failure mechanisms, Γ_R and Σ_R. Colored regions indicate active failure mechanism at the critical value of misfit stress.

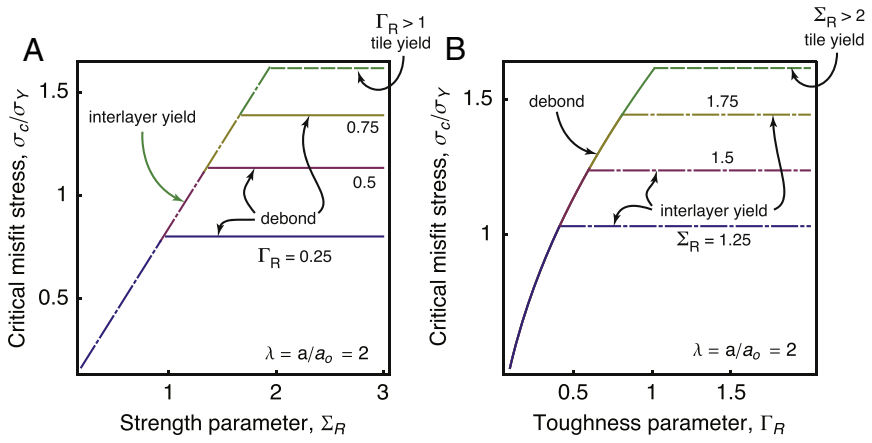

Fig. 6. Critical misfit stress σ_c/σ_Y as a function of the material parameters Σ_R and Γ_R for fixed tile size $\lambda = a/a_o = 2$, determined by the minimum value required to trigger any mechanism. The line pattern indicates the active failure mechanism at the critical misfit stress.

indicates that this failure mode is less likely, as it is moved further from the application point.

The lower corner of the "tile yielding" space represents the minimum combination of (Σ_R, Γ_R) that will avoid all three failure mechanisms for that tile size, provided the actual misfit strains are set equal to the critical ones at that size. Put another way, given lower bounds on the material parameters, the intersection of the three regions indicates the maximum allowable misfit stress for a given tile size. One can solve for the intersection point using the solutions above, and generate a single plot that illustrates the maximum possible critical strain for a given tile size, and the associated lower bounds on the properties needed for design (Fig. 8).

This figure can be used to rapidly identify the active constraint and maximum allowable tile size for a set of properties. For example, consider the case where the design requires that the allowable misfit stress is $\sigma_c = 5\sigma_Y$. The maximum tile size that can be used is $\lambda = 0.8$, *provided* the interface toughness yields at least $\Gamma_R = 4.5$, and the interlayer yield strength produces at least $\Sigma_R = 3$. As a second example, suppose materials are chosen such that $\Gamma_R = 2$, and $\Sigma_R = 5$. A tile size of $\lambda = 0.5$ avoids interlayer yielding at the maximum possible misfit stress, but at that size, Γ_R is less than the minimum required (i.e. the minimum Γ_R at that size is 7). For the tile size $\lambda = 1.5$, which corresponds to the maximum for the given Γ_R, the required Σ_R is less than that stated for the problem, so this size is acceptable. Thus, for this example interface debonding is the active constraint, and $\lambda = 1.5$ is the maximum possible tile size, provided the misfit stress is equal to the maximum possible at this size.

Finally, as an illustration of the underlying scaling implied by the models, consider a model system comprising a 0.2 mm thick tile with $(E_f, \nu_f) = (200\,\text{GPa}, 0.2)$ bonded to a substrate with a 0.02 mm thick interlayer with $(E_i, \nu_i) = (4\,\text{GPa}, 0.4)$. (This is consistent with a ceramic feature bonded with epoxy to the substrate.) The characteristic shear transfer length in this case is $a_o \sim 0.8$ mm, and one can expect the present shear lag model to be accurate for tile sizes at least five times the thickness, or ~1 mm: this implies the present models are accurate for $\lambda \geq \sim 1.3$. Fig. 2 reveals that the present model (accurately) predicts stresses in the range of 25–100% of the blanket film result, thus illustrating that the shear lag model is applicable for meaningful tile sizes, in a regime where the finite-sized tile result is very different from the blanket film result. A similar but more macroscopic example is a 1 cm thick steel tile used to spread head, bonded with a thicker polymer layer for thermal insulation 1 mm thick, yields $a_o \sim 3.8$ cm, again with $\lambda_{min} = 1.3$. For this application, the model applies for tiles greater than 5 cm, for which the stresses are again 25% of the infinite tile result.

4. Conclusion

Closed-form analytical solutions have been presented for the stresses and displacements of an axisymmetric tile bonded with a

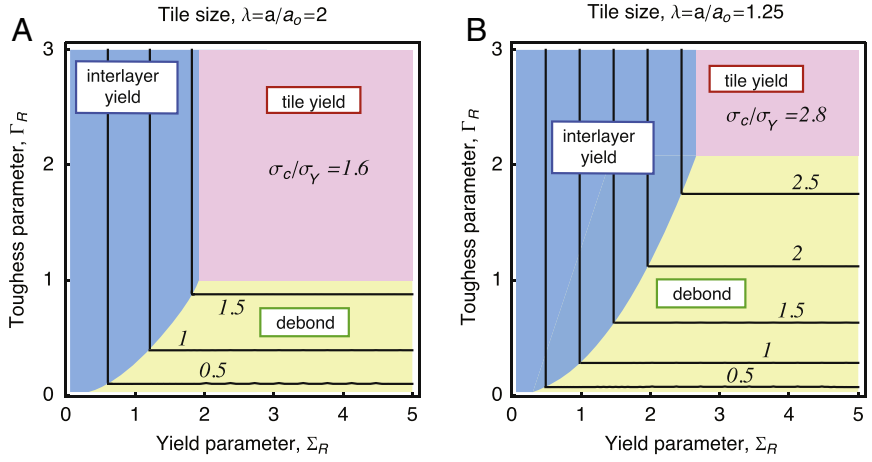

Fig. 7. Contours of the critical misfit stress, σ_o^c/σ_Y and the material parameters controlling various failure mechanisms (Γ_R and Σ_R) for fixed tile sizes. Colored regions indicate active failure mechanism at the critical value of misfit stress.

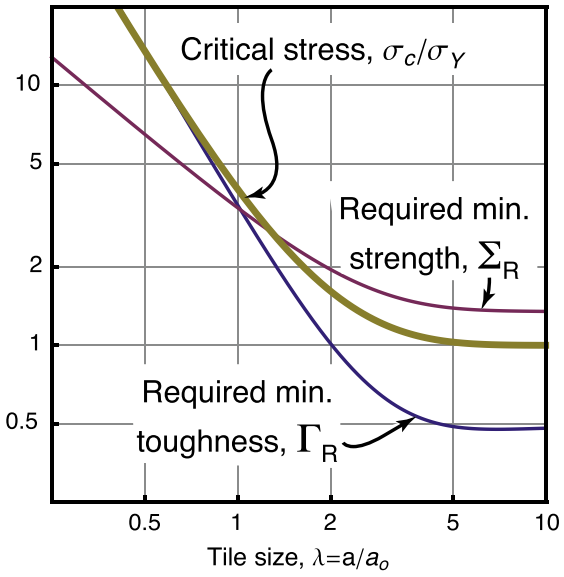

Fig. 8. Maximum possible critical misfit stress as a function of tile size, and the associated required minimum values of the material parameters Γ_R and Σ_R.

compliant interlayer to a substrate. The analysis enables predictions for the energy release-rates associated with a convergent delamination front that moves from the outer edge inwards. The solutions can be utilized to construct failure mechanism maps, which indicate active failure mechanisms as a function of material properties and tile size. The solutions indicate that failure mechanisms depend on the single sizing parameter $\lambda = a/a_o$, that incorporates material and geometric information to describe the length-scale over which shear transfer occurs. Together with λ, two key dimensionless parameters are presented that control the transitions from one mechanism to another: these are essentially measures of the relative importance of the interface fracture toughness to tile yield strength, and the interlayer shear strength relative to the tile yield strength. Taken together, the solutions and key scaling factors provide a broad basis for tiling system design.

Acknowledgments

MRB gratefully acknowledges the support of the National Science Foundation through CMII Grant No. #1063714 (formerly #0800790).

References

[1] R.S. Dahiya, G. Metta, M. Valle, A. Adami, L. Lorenzelli, Appl. Phys. Lett. 95 (2009) 034105.
[2] Y. Sano, K. Nunomara, N. Koyama, H. Sakuma, K. Utsumi, IEEE Trans. Electron Dev. 33 (1986) 1155.
[3] S. Zamir, B. Meyler, J. Salzman, Appl. Phys. Lett. 78 (2001) 288.
[4] Y. Feng, L. Wu, Int. J. Sol. Struct. 38 (2001) 1551.
[5] T. Mahaboonpachai, Y. Kuromiya, T. Matsumoto, Construct. Build. Mater. 22 (2008) 2001.
[6] R.J. Harries, S.K. Sitaraman, IEEE Trans. Comp. Pack. Tech. 24 (2001) 256.
[7] R.D. Watson, J. Nucl. Mater. 176 (177) (1990) 110.
[8] J.P. Blanchard, J.D. Watson, Nucl. Eng. Des. 4 (1986) 61.
[9] D.W. Lee, Y.D. Bae, S.K. Kim, B.G. Hong, H.K. Jung, J.Y. Park, Y.H. Jeon, Y.H.B.K. Choi, Fusion Eng. Des. 84 (2009) 1160.
[10] T. Kundu, R. Reibel, K. Jata, Proc. SPIE 6177 (2006) 617705.
[11] H.-H. Yu, J.W. Hutchinson, Thin Solid Films 423 (2003) 54.
[12] S.P. Lacour, S. Wagner, R.J. Narayan, T. Li, Z. Suo, J. Appl. Physiol. 100 (2006) 014913.
[13] P.I. Hsu, M. Huang, Z. Xi, S. Wagner, Z. Suo, J.C. Sturm, J. Appl. Physiol. 95 (2004) 705.
[14] N. Lu, J. Yoon, Z. Suo, Int. J. Mater. Res. 98 (2007) 717.
[15] J.Y. Sun, N. Lu, J. Yoon, K.-H. Oh, Z. Suo, J.J. Vlassak, J. Appl. Physiol. 111 (2012) 031517.
[16] H.L. Cox, Br. J. Appl. Phys. 3 (1952) 72.
[17] S.R. Swanson, J. Eng. Mater. Tech. 111 (1989) 145.
[18] J.H. Selverian, D. O'Neil, Thin Solid Films 235 (1993) 120.
[19] K. Nakasa, S. Takata, H. Ichigo, Eng. Frac. Mech. 59 (1998) 191.
[20] M. Yanaka, Y. Tsukahara, N. Nakaso, N. Takeda, J. Mater. Sci. 33 (1998) 2111.
[21] M. Yanaka, Y. Kato, Y. Tsukahara, N. Takeda, Thin Solid Films 355–356 (1999) 347.
[22] J. Liang, R. Huang, H. Yin, J.C. Sturm, K.D. Hobart, Z. Suo, Acta Mater. 50 (2002) 2933.
[23] J. Andersons, Y. Leterrier, I. Fescenko, Thin Solid Films 434 (2003) 203.
[24] J. Andersons, Y. Leterrier, G. Tornare, P. Dumont, J.-A.E. Manson, Mech. Mat. 39 (2007) 834.
[25] Z.C. Xia, J.W. Hutchinson, J. Mech. Phys. Sol. 48 (2000) 1107.
[26] J.W. Hutchinson, Z. Suo, Adv. Appl. Mech. 29 (1992) 63.
[27] L.B. Freund, S. Suresh, Thin Film Materials, Cambridge University Press, Cambridge, England, 2003.
[28] H.H. Yu, M.Y. He, J.W. Hutchinson, Acta Mater. 49 (2001) 93.
[29] M.D. Thouless, Acta Metall. Mater. 36 (1988) 3131.
[30] M.Y. He, A.G. Evans, J.W. Hutchinson, Acta Mater. 8 (1997) 3481.
[31] J.-Y. Sun, N. Lu, J. Yoon, K.-H. Oh, Z. Suo, J.J. Vlassack, J. Mater. Res. 24 (2009) 3338.